Inorganic Chemistry

Article

pubs.acs.org/IC

Di-μ-oxo Dimetal Core of Mn^{IV} and Ti^{IV} as a Linker Between Two Chiral Salen Complexes Leading to the Stereoselective Formation of Different *M*- and *P*-Helical Structures

Takuya Kurahashi,[†] Masahiko Hada,[‡] and Hiroshi Fujii*[,†]

[†]Institute for Molecular Science and Okazaki Institute for Integrative Bioscience, National Institutes of Natural Sciences, Myodaiji, Okazaki, Aichi 444-8787, Japan

[‡]Department of Chemistry, Graduate School of Science, Tokyo Metropolitan University, 1-1 Minami-Osawa, Hachioji-shi, Tokyo 192-0397, Japan

Supporting Information

ABSTRACT: Because of restricted rotational freedom along the metal−metal axis, a di-μ-oxo dimetal core could be an excellent building block to create dinuclear compounds with well-defined stereochemistry, but their stereoselective synthesis remains a challenge. We herein report the formation of di-μ-oxo dimanganese(IV) complexes with tetradentate salen ligands bearing different degrees of steric bulk, in order to study stereochemical aspects of the dimerization reaction that potentially generates multiple stereoisomers. X-ray crystallography shows that the di-μ-oxo dimanganese(IV) complex with salen, where salen is (*R*,*R*)-*N*,*N*′-bis(3,5-di-*tert*-butylsalicylidene)-1,2-cyclohexanediamine, adopts a unique structure in which two salen complexes are arranged in an *M*-helical fashion. According to the solution study using ^{1}H, ^{2}H NMR, and circular dichroism spectroscopies, the dimerization reaction is highly diastereoselective in the presence of the *tert*-butyl group at the 3/3′ position as a determinant steric factor. In contrast, the di-μ-oxo dititanium(IV) complex with the same salen ligand was previously reported to afford an opposite *P*-helical dimer. The present DFT study clarifies that a less-covalent Ti−O bonding causes a distortion of the di-μ-oxo dititanium(IV) core structure, generating a completely different framework for interligand interaction. The present study provides a solid basis to understand the stereochemistry for the formation of the di-μ-oxo dimetal core.

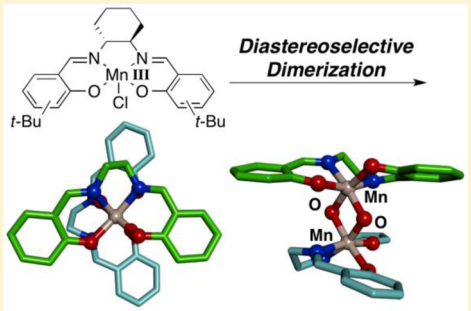

INTRODUCTION

Di-μ-oxo dimetal cores commonly found in metalloenzymes have attracted considerable attention as a structural motif to create artificial small-molecular systems. The most prominent feature of di-μ-oxo dimetal cores is a significantly short metal−metal separation. Strong magnetic interactions between two paramagnetic metal centers induce characteristic spectroscopic properties, and those of di-μ-oxo dimanganese(IV) complexes are extensively investigated in relation to the oxygen-evolving complex of photosystem II and manganese catalases.[1−4] The unique structural feature of di-μ-oxo dimetal cores is also a key for distinct oxygenation reactivity, most remarkably in the case of di-μ-oxo dicopper and diiron complexes.[5−8]

Another promising feature of di-μ-oxo dimetal cores is their stereochemical rigidity that arises from restricted rotational freedom along the metal−metal axis, in contrast to single-bridging linkers. Owing to this feature, the di-μ-oxo dimetal motif generates multiple stereoisomers upon the dimerization of two mononuclear units, creating stereochemical diversity for dinuclear coordination compounds. Rich stereochemistry could potentially expand the functionality of coordination compounds, although stereochemical aspects of the di-μ-oxo dimetal core have received less attention. Over the past two decades, the control of stereogenic metal centers in coordination compounds has been the subject of intense research, as described in several review papers.[9−14] A number of different approaches are now being developed.[15−26] However, stereoselective synthesis of polynuclear coordination compounds still remains a challenge, as compared with the state-of-the-art synthesis of organic compounds with multiple chiral centers.

We herein report the formation of $[Mn^{IV}(salen)]_2(O)_2$ (di-μ-oxo dimanganese(IV) salen) complexes bearing different degrees of steric bulk. Salen and related ligands, which are readily prepared from diamines and salicylaldehydes, are widely utilized as catalysts and materials, because of the ease to modulate their steric and electronic properties.[27−30] We utilized sterically demanding salen ligands bearing (*R*,*R*)-*trans*-cyclohexane-1,2-diamine as a common chiral unit (Chart 1). Although the preparation of di-μ-oxo dimanganese(IV) complexes with salen ligands was previously reported,[31−35] the incorporation of such steric bulk and chirality has been unexplored. The present study shows that, while the dimerization of the manganese complex with L-5-*t*-Bu affords a mixture of diastereomers, the assembly of

Received: October 10, 2013
Published: January 8, 2014

   dx.doi.org/10.1021/ic402572h | *Inorg. Chem.* 2014, 53, 1070−1079

Chart 1. Salen Ligands Utilized in This Study and Their Abbreviations

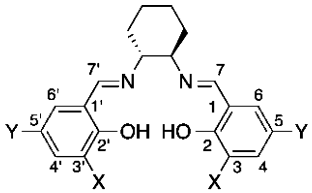

manganese complexes with L-3,5-*t*-Bu and L-3-*t*-Bu is highly diastereoselective to give one of two diastereomers. Quite interestingly, the present results are apparently different from the stereochemistry upon the formation of the di-μ-oxo dititanium(IV) core with salen and related ligands,[36−46] and the opposite diastereomer is obtained in spite of the use of the same chiral salen ligand.[36,37,40] The present study clarifies that the di-μ-oxo dimetal core structure is significantly altered between manganese(IV) and titanium(IV) as a consequence of the electronic difference of metal−oxygen bonding, generating completely different frameworks for interligand interaction. The present study provides a solid basis to understand the stereochemistry for the formation of the di-μ-oxo dimetal core.

RESULTS AND DISCUSSION

X-ray Crystal Structure of $[Mn^{IV}(L\text{-}3,5\text{-}t\text{-}Bu)]_2(O)_2$. The $[Mn^{IV}(L\text{-}3,5\text{-}t\text{-}Bu)]_2(O)_2$ complex was readily prepared in 71% yield by air oxidation upon washing the toluene solution of $Mn^{III}(L\text{-}3,5\text{-}t\text{-}Bu)(Cl)$ with aqueous KOH solution. Precipitation in hot acetonitrile affords the pure sample, and elemental analysis shows that its composition is consistent with $[Mn^{IV}(L\text{-}3,5\text{-}t\text{-}Bu)]_2(O)_2$. According to the ESI (electrospray ionization) mass spectrometry, the product shows a main signal at m/z 1231.72, and the isotope distribution pattern of this signal is in agreement with the calculation for $[Mn^{IV}(L\text{-}3,5\text{-}t\text{-}Bu)]_2(O)_2 + H^+$ (Figure S1, Supporting Information, SI).

Figure 1 shows the X-ray crystal structure of $[Mn^{IV}(L\text{-}3,5\text{-}t\text{-}Bu)]_2(O)_2$. The crystallographic data are summarized in Table S1 (SI). The $[Mn^{IV}(L\text{-}3,5\text{-}t\text{-}Bu)]_2(O)_2$ complex adopts a highly symmetric structure where one mononuclear unit is exactly identical to the other. The structural parameters are summarized in Table 1. The Mn−N2 bond that is trans to the bridging O4 atom is significantly elongated by 0.095 Å as compared to the Mn−N1 bond. This structural feature is also observed for another di-μ-oxo dimanganese(IV) complex with the related ligand bearing the propane-1,3-diamine instead of *trans*-cyclohexane-1,2-diamine, reported by Pecoraro et al.[35] The Mn−O1 bond that is trans to the bridging O3 atom is longer by 0.025 Å than the Mn−O2 bond. The Mn−O3 bond that is trans to the phenolic O1 atom is also elongated by 0.023 Å as compared to the Mn−O4 bond. However, these structural features are not evident for Pecoraro's di-μ-oxo dimanganese(IV) complex. The Mn−Mn distance increases from 2.7753 Å for Pecoraro's di-μ-oxo dimanganese(IV) complex to 2.7853 Å for sterically demanding $[Mn^{IV}(L\text{-}3,5\text{-}t\text{-}Bu)]_2(O)_2$.

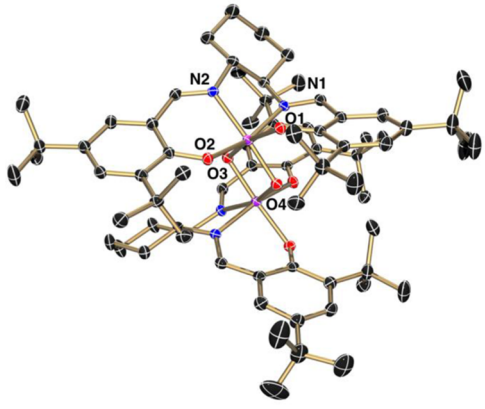

Figure 1. X-ray crystal structure of $[(R,R)\text{-}Mn^{IV}(L\text{-}3,5\text{-}t\text{-}Bu)]_2(O)_2$. Thermal ellipsoids represent the 50% probability surface. Hydrogen atoms are omitted for the sake of clarity.

Table 1. Selected Structural Parameters for $[Mn^{IV}(L\text{-}3,5\text{-}t\text{-}Bu)]_2(O)_2$

	$[Mn(L\text{-}3,5\text{-}t\text{-}Bu)]_2(O)_2$
Mn−O1/Å	1.9450(15)
Mn−O2/Å	1.9201(16)
Mn−N1/Å	1.9834(17)
Mn−N2/Å	2.0783(18)
Mn−O3/Å	1.8323(13)
Mn−O4/Å	1.8096(13)
Mn−Mn/Å	2.7853(6)
O1−Mn−O3/deg	167.51(7)
O1−Mn−O4/deg	87.75(7)
O2−Mn−O3/deg	98.83(5)
O2−Mn−O4/deg	100.15(5)
N1−Mn−O3/deg	91.47(5)
N1−Mn−O4/deg	95.90(5)
N2−Mn−O3/deg	83.88(7)
N2−Mn−O4/deg	163.00(7)
Mn−O3−Mn′/deg	98.93(10)
Mn−O4−Mn′/deg	100.63(10)

The X-ray structure in Figure 1 also shows that the (*R*,*R*)-*trans*-cyclohexane-1,2-diamine stereodirecting group commonly induces the *cis*-β-Δ configuration[47] around both manganese centers. Two mononuclear units with the same *cis*-β-Δ configuration are then connected with the di-μ-oxo linkage, generating a twist between two manganese salen complexes. Figure 2 illustrates the twist of the two manganese salen complexes in $[Mn^{IV}(L\text{-}3,5\text{-}t\text{-}Bu)]_2(O)_2$, which forms an *M*-helical structure. The formation of *M*-helical $[Mn^{IV}(L\text{-}3,5\text{-}t\text{-}Bu)]_2(O)_2$ is highly diastereoselective, as shown by solution studies described in the next section. Quite interestingly, previously reported X-ray crystal structures of $[Ti^{IV}(salen)]_2(O)_2$ complexes, where salen is L-3-*t*-Bu or (*R*,*R*)-*N*,*N*′-bis(salicylidene)-1,2-cyclohexanediamine, show the opposite *P*-helical structure.[36,40] It was reported that the solution of $[Ti^{IV}(salen)]_2(O)_2$ contains an equilibrium between the dimeric $[Ti^{IV}(salen)]_2(O)_2$ and the monomeric species, but the ^1H NMR spectra are indicative of a single diastereomer for the dimeric $[Ti^{IV}(salen)]_2(O)_2$.[39] The (*R*,*R*)-*trans*-cyclohexane-1,2-diamine moiety induces the *cis*-β-Δ configuration around the titanium in $[Ti^{IV}(L\text{-}3\text{-}t\text{-}Bu)]_2(O)_2$, just as observed for $[Mn^{IV}(L\text{-}3,5\text{-}t\text{-}Bu)]_2(O)_2$. However, the subsequent formation of the di-μ-oxo dimetal core produces diastereomeric *M*- and *P*-helical structures for $[Mn^{IV}(L\text{-}3,5\text{-}t\text{-}Bu)]_2(O)_2$ and $[Ti^{IV}(L\text{-}3\text{-}t\text{-}Bu)]_2(O)_2$, respectively.

dx.doi.org/10.1021/ic402572h | Inorg. Chem. 2014, 53, 1070−1079

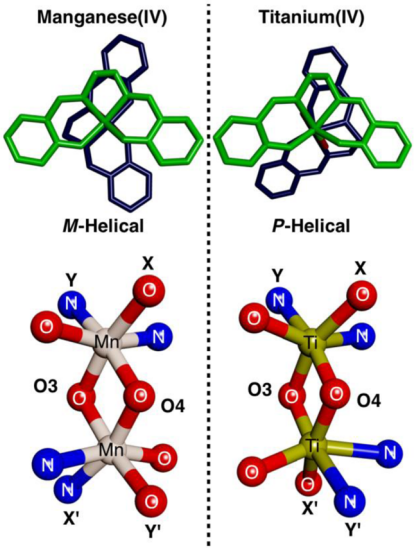

Figure 2. *M*- and *P*-helical structures in $[Mn^{IV}(L\text{-}3,5\text{-}t\text{-}Bu)]_2(O)_2$ and $[Ti^{IV}(L\text{-}3\text{-}t\text{-}Bu)]_2(O)_2$ bearing (*R*,*R*)-*trans*-cyclohexane-1,2-diamine as a common chiral unit.

The diastereomeric *M*- and *P*-helical di-μ-oxo dimetal complexes differ in the configuration of the di-μ-oxo dimetal core (Figure 2). In the case of *M*-helical $[Mn^{IV}(L\text{-}3,5\text{-}t\text{-}Bu)]_2(O)_2$, the bridging O3 atom occupies the position trans to the phenolic O1 and O1′ atoms, while the bridging O4 atom is trans to the imine N2 and N2′ atoms. In contrast, the bridging O atom in *P*-helical $[Ti^{IV}(L\text{-}3\text{-}t\text{-}Bu)]_2(O)_2$ is trans to the phenolic O and imine N atom for both O3 and O4. We then compared the structural parameters of di-μ-oxo dimanganese(IV) and dititanium(IV) complexes in detail (Table 2). The metal−

Table 2. Comparison of the Structural Parameters of the Di-μ-oxo Dimetal Cores

	$[Mn^{IV}(L\text{-}3,5\text{-}t\text{-}Bu)]_2(O)_2$	$[Ti^{IV}(L\text{-}3\text{-}t\text{-}Bu)]_2(O)_2$[a]
M−M/Å	2.7853	2.8122
X−M−O/deg	167.51	144.85
X′−M−O/deg	163.00	155.64
Y−M−O/deg	163.00	157.11
Y′−M−O/deg	167.51	164.56

[a]Structural parameters of $[Ti^{IV}(L\text{-}3\text{-}t\text{-}Bu)]_2(O)_2$ are adopted from ref 40.

metal separation, which is a critical structural factor for the steric interaction between two mononuclear units, is more elongated for $[Ti^{IV}(L\text{-}3\text{-}t\text{-}Bu)]_2(O)_2$ by 0.0269 Å than for $[Mn^{IV}(L\text{-}3,5\text{-}t\text{-}Bu)]_2(O)_2$. In addition, the X(X′)−M−O and Y(Y′)−M−O angles are more deviated from the ideal angle of 180° for $[Ti^{IV}(L\text{-}3\text{-}t\text{-}Bu)]_2(O)_2$ than for $[Mn^{IV}(L\text{-}3,5\text{-}t\text{-}Bu)]_2(O)_2$.

Solution Studies. To investigate whether the dimerization of (*R*,*R*)-$Mn^{III}(L\text{-}3,5\text{-}t\text{-}Bu)(Cl)$ selectively affords an *M*-helical dimer or gives a diastereomeric mixture of *M*- and *P*-helical dimers, we measured the ^{1}H NMR spectrum of $[Mn^{IV}(L\text{-}3,5\text{-}t\text{-}Bu)]_2(O)_2$, along with ^{2}H NMR spectra of selectively deuterated di-μ-oxo dimanganese(IV) complexes with L-3,5-*t*-Bu-d_4 and L-3,5-*t*-Bu-d_2 for the purpose of assigning the ^{1}H NMR signals (Chart 2). In L-3,5-*t*-Bu-d_4, ^{2}H atoms are selectively incorporated into the phenolate rings (80% D) and the *tert*-butyl groups (7% D). In L-3,5-*t*-Bu-d_2, the 7/7′ position of the azomethine group is selectively deuterated (99.5% D). The ^{1}H NMR spectrum of the

Chart 2. Selectively Deuterated Salen Ligands and Their Abbreviations[a]

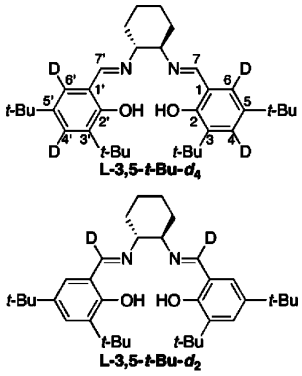

[a]In L-3,5-*t*-Bu-d_4, ^{2}H atoms are selectively incorporated into the phenolate rings (80% D) and the *tert*-butyl groups (7% D). In L-3,5-*t*-Bu-d_2, the 7/7′ position of the azomethine group is selectively deuterated (99.5% D).

crude sample without purification shows only the same set of signals in addition to the free ligand as a byproduct (Figure S2, SI).

The $[Mn^{IV}(L\text{-}3,5\text{-}t\text{-}Bu)]_2(O)_2$ complex shows relatively sharp signals at 8.8, 8.3, 6.4, and 4.3 ppm, which are unambiguously assigned as arising from the phenolate protons (Figure 3). The

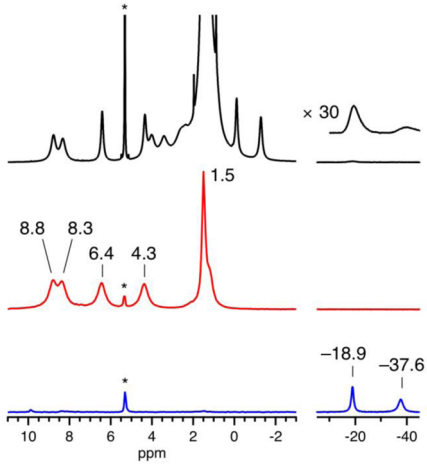

Figure 3. ^{1}H NMR spectrum of 10 mM solution of $[Mn^{IV}(L\text{-}3,5\text{-}t\text{-}Bu)]_2(O)_2$ in CD_2Cl_2 at 298 K (black line). ^{2}H NMR spectra of 20 mM solution of $[Mn^{IV}(L\text{-}3,5\text{-}t\text{-}Bu\text{-}d_4)]_2(O)_2$ (red line) and $[Mn^{IV}(L\text{-}3,5\text{-}t\text{-}Bu\text{-}d_2)]_2(O)_2$ (blue line) in CH_2Cl_2 at 298 K. The signals denoted with asterisks come from residual $CHDCl_2$ and are referenced to 5.32 ppm.

azomethine protons are observed at −18.9 and −37.6 ppm as a broad signal. Upon decreasing the temperature, the azomethine signals move downfield to −12.2 and −24.8 ppm at 193 K (Figure S3, SI), which is indicative of the antiferromagnetic coupling between two manganese(IV) centers. A set of four phenolate and two azomethine signals in solution is in agreement with the solid-state structure of $[Mn^{IV}(L\text{-}3,5\text{-}t\text{-}Bu)]_2(O)_2$. In addition, other minor signals are not observed at all, indicating that the solution contains only one diastereomer. Thus, the dimerization reaction of $Mn^{III}(L\text{-}3,5\text{-}t\text{-}Bu)(Cl)$ affords *M*-helical $[Mn^{IV}(L\text{-}3,5\text{-}t\text{-}Bu)]_2(O)_2$ in a highly diastereoselective manner. We also measured NMR spectra of *M*-helical $[Mn^{IV}(L\text{-}3,5\text{-}t\text{-}Bu)]_2(O)_2$ in toluene-d_8 at higher temperature in the range from

dx.doi.org/10.1021/ic402572h | Inorg. Chem. 2014, 53, 1070−1079

298 to 363 K (Figure S4, SI), but we did not observe any sign of the thermal interconversion between *M*- and *P*-helical $[Mn^{IV}(L\text{-}3,5\text{-}t\text{-}Bu)]_2(O)_2$ even at 363 K. To investigate a possible equilibrium between monomeric and dimeric species, the toluene solution of $[Mn^{IV}(L\text{-}3,5\text{-}t\text{-}Bu)]_2(O)_2$ and $[Mn^{IV}(L\text{-}3,5\text{-}t\text{-}Bu\text{-}d_4)]_2(O)_2$ was stirred at room temperature for 2 days. However, ESI mass spectrometry showed no exchange reaction between the Mn(L-3,5-*t*-Bu) and Mn(L-3,5-*t*-Bu-d_4) moieties (Figure S5, SI), indicating that a monomeric manganese species is not formed at all in solution, in contrast to the $[Ti^{IV}(salen)]_2(O)_2$ complexes.[39,44]

The solution conformation of $[Mn^{IV}(L\text{-}3,5\text{-}t\text{-}Bu)]_2(O)_2$ was then investigated by CD spectroscopy, which is a powerful technique for stereochemical analysis.[48,49] The $[(R,R)\text{-}Mn^{IV}(L\text{-}3,5\text{-}t\text{-}Bu)]_2(O)_2$ shows intense characteristic CD signals of positive and negative sign at 226 and 255 nm (Figure 4), which

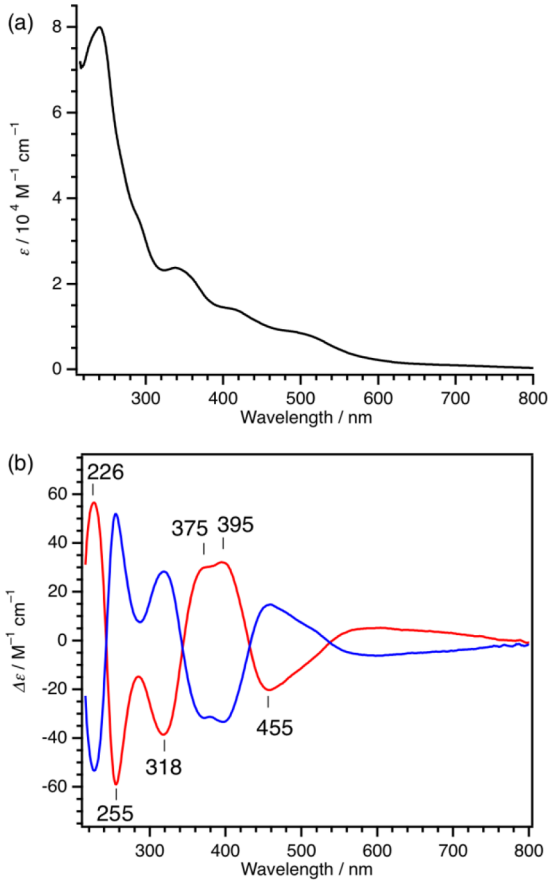

Figure 4. (a) Absorption spectrum of $[(R,R)\text{-}Mn^{IV}(L\text{-}3,5\text{-}t\text{-}Bu)]_2(O)_2$ in CH_2Cl_2 at 298 K (0.3 mM, 0.05 cm cell). (b) CD spectra of $[(R,R)\text{-}Mn^{IV}(L\text{-}3,5\text{-}t\text{-}Bu)]_2(O)_2$ (red line) and $[(S,S)\text{-}Mn^{IV}(L\text{-}3,5\text{-}t\text{-}Bu)]_2(O)_2$ (blue line) in CH_2Cl_2 at 298 K (0.3 mM, 0.05 cm cell).

are most probably assigned as arising from the distortion of the salen ligand.[50] As previously reported, the $Mn^{IV}(L\text{-}3,5\text{-}t\text{-}Bu)(X)_2$ complexes (X = OI(Cl)Ph, OCH_2CF_3, and N_3), which adopt a chirally distorted stepped conformation, commonly induce an intense CD absorption of a negative sign around 275 nm ($\Delta\varepsilon$ = −50 to −60 M^{-1} cm^{-1}) for (*R*,*R*)-enantiomer, while the corresponding CD absorption of $Mn^{IV}(L\text{-}3,5\text{-}t\text{-}Bu)(Cl)_2$ with a flat conformation is considerably weaker ($\Delta\varepsilon$ = ∼−20 M^{-1} cm^{-1}).[50−52] Thus, the intense CD absorption for the $[Mn^{IV}(L\text{-}3,5\text{-}t\text{-}Bu)]_2(O)_2$ is indicative of a chirally distorted conformation also in solution.

To investigate the exact factor for the diastereoselective formation of *M*-helical $[Mn^{IV}(L\text{-}3,5\text{-}t\text{-}Bu)]_2(O)_2$, we alternately removed the *tert*-butyl groups at the 3/3′ and 5/5′ positions and prepared the L-3-*t*-Bu and L-5-*t*-Bu ligands (Chart 1). The $[Mn^{IV}(L\text{-}3\text{-}t\text{-}Bu)]_2(O)_2$ complex was successfully prepared from $Mn^{III}(L\text{-}3\text{-}t\text{-}Bu)(Cl)$ in the same manner except for the use of the solvent mixture of toluene and dichlormethane (3:1) because of low solubility. The ^1H NMR spectrum of the crude sample shows the formation of the free ligand as a byproduct (Figure S2, SI). To remove a trace amount of the free ligand, HPLC (high-performance liquid chromatography) was utilized to obtain an analytically pure sample. Only one diastereomer was found with the HPLC purification. The ESI mass spectrum of $[Mn^{IV}(L\text{-}3\text{-}t\text{-}Bu)]_2(O)_2$ gives a main signal at *m*/*z* 1007.46, which arises from the $[Mn^{IV}(L\text{-}3\text{-}t\text{-}Bu)]_2(O)_2 + H^+$ ion (Figure S6, SI). The ^1H NMR spectrum of $[Mn^{IV}(L\text{-}3\text{-}t\text{-}Bu)]_2(O)_2$ (Figure 5b) is almost

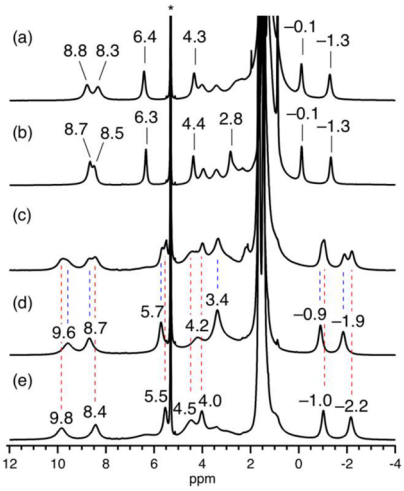

Figure 5. ^1H NMR spectra of (a) $[Mn^{IV}(L\text{-}3,5\text{-}t\text{-}Bu)]_2(O)_2$, (b) $[Mn^{IV}(L\text{-}3\text{-}t\text{-}Bu)]_2(O)_2$, and (c) $[Mn^{IV}(L\text{-}5\text{-}t\text{-}Bu)]_2(O)_2$ in CD_2Cl_2 at 298 K (10 mM). ^1H NMR spectra of (d) *P*-helical $[Mn^{IV}(L\text{-}5\text{-}t\text{-}Bu)]_2(O)_2$ and (e) *M*-helical $[Mn^{IV}(L\text{-}5\text{-}t\text{-}Bu)]_2(O)_2$ in CD_2Cl_2 at 298 K (10 mM). The signals denoted with an asterisk come from residual $CHDCl_2$ and are referenced to 5.32 ppm.

identical to that of $[Mn^{IV}(L\text{-}3,5\text{-}t\text{-}Bu)]_2(O)_2$ except for the signal at 2.8 ppm, which is assigned as arising from the phenolate protons at the 5/5′ position. The CD spectrum of $[Mn^{IV}(L\text{-}3\text{-}t\text{-}Bu)]_2(O)_2$ is essentially the same as that of $[Mn^{IV}(L\text{-}3,5\text{-}t\text{-}Bu)]_2(O)_2$ (Figure S7, SI). These data clearly show that the dimerization reaction of $Mn^{III}(L\text{-}3\text{-}t\text{-}Bu)(Cl)$ selectively affords *M*-helical $[Mn^{IV}(L\text{-}3\text{-}t\text{-}Bu)]_2(O)_2$, which is exactly the same as observed for $[Mn^{IV}(L\text{-}3,5\text{-}t\text{-}Bu)]_2(O)_2$.

In sharp contrast, the dimerization of $Mn^{III}(L\text{-}5\text{-}t\text{-}Bu)(Cl)$ affords a mixture of two species, as clearly seen from the ^1H NMR spectrum of the sample after the removal of the free ligand byproduct (Figure 5c). The ^1H NMR spectrum of the crude sample before purification is shown in Figure S2 (SI). These two species are successfully separated with HPLC. As shown in d and e of Figure 5, the ^1H NMR spectra of these two species are quite similar, and the spectral patterns are both in agreement with the formation of $[Mn^{IV}(L\text{-}5\text{-}t\text{-}Bu)]_2(O)_2$. Analytical data of purified samples are both consistent with the $[Mn^{IV}(L\text{-}5\text{-}t\text{-}Bu)]_2(O)_2$ composition. ESI mass spectrometry shows that the samples shown in d and e of Figure 5 give a single ion signal at *m*/*z*

dx.doi.org/10.1021/ic402572h | Inorg. Chem. 2014, 53, 1070−1079

1007.37 and 1007.47, respectively, which is exactly the value for the $[Mn^{IV}(L\text{-}5\text{-}t\text{-}Bu)]_2(O)_2 + H^+$ ion (Figure S8, SI). Thus, both of these species are reliably assigned as a $[Mn^{IV}(L\text{-}5\text{-}t\text{-}Bu)]_2(O)_2$ complex. These two species show almost the same absorption spectra (Figure 6a). However, the CD spectra of these two species are substantially different (Figure 6b). The CD spectrum shown in red is essentially the same as those of *M*-helical $[Mn^{IV}(L\text{-}3,5\text{-}t\text{-}Bu)]_2(O)_2$ and $[Mn^{IV}(L\text{-}3\text{-}t\text{-}Bu)]_2(O)_2$, indicative of the formation of the same *M*-helical dimer. The CD spectrum in blue shows weaker signals at 218 and 307 nm, indicative of the formation of the opposite *P*-helical dimer. A CD spectrum of $[Mn^{IV}(salen)]_2(O)_2$ is the sum of two CD signals. One of the signals arises from the mononuclear unit with a chirally distorted *cis*-β-Δ configuration, which is exactly the same for *M*- and *P*-helical dimers. As previously reported, monomeric salen complexes with chirally distorted stepped conformation show CD signals of comparable intensity.[50,51] The other signals come from the exciton coupling between two salen ligands that are arranged in an *M*- or *P*-helical fashion.[53] The differences of CD signals for *M*- or *P*-helical dimers are only minute, probably because the contribution of the latter origin is relatively small.

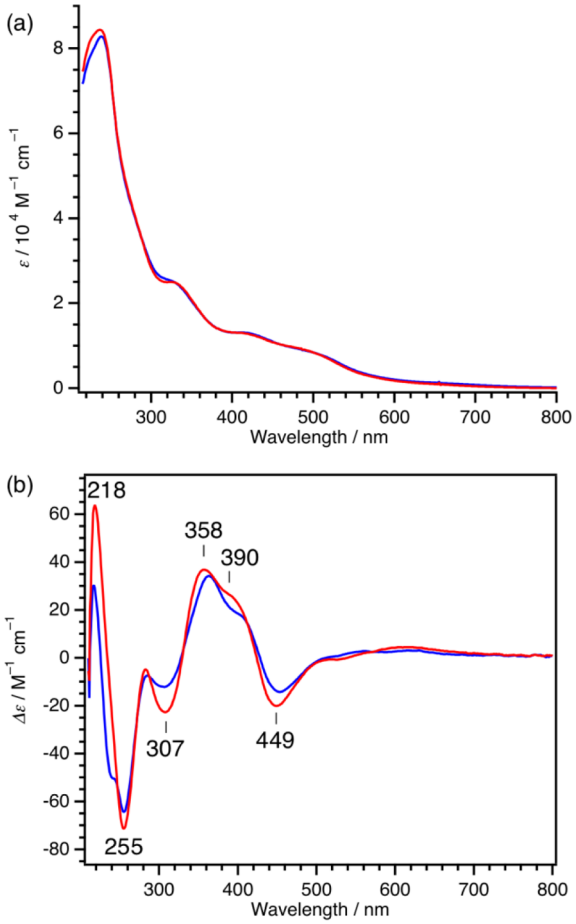

Figure 6. (a) Absorption and (b) CD spectra of *P*-helical $[(R,R)\text{-}Mn^{IV}(L\text{-}5\text{-}t\text{-}Bu)]_2(O)_2$ (blue line) and (e) *M*-helical $[(R,R)\text{-}Mn^{IV}(L\text{-}5\text{-}t\text{-}Bu)]_2(O)_2$ (red line) in CH_2Cl_2 at 298 K (0.3 mM, 0.05 cm cell).

The effect of reaction conditions on the selectivity between *M*- and *P*-helical dimers is investigated. The ratios of *M*- and *P*-helical dimers are estimated by curve fittings of the ^{1}H NMR signals (Figure S9, SI). The reaction of $Mn^{III}(L\text{-}5\text{-}t\text{-}Bu)(Cl)$ in CH_2Cl_2 with aqueous KOH solution at 25 °C gives the mixture of *M*- and *P*-helical dimers (1:0.61), which is slightly altered to the ratio of 1:0.47 when the reaction is run at −10 °C. The use of NaOH instead of KOH has negligibly small effect (1:0.51). The solvent polarity alters the ratio between *M*- and *P*-helical dimers; 1:0.85 in CH_2Cl_2 and diethylether (7:3), 1:0.35 in CH_2Cl_2 and hexane (1:1). However, under any conditions, the *M*-helical dimer could not be obtained selectively, indicating that the 3/3′-*tert*-butyl group is exactly the key factor for the diastereoselective formation of *M*-helical $[Mn^{IV}(L\text{-}3,5\text{-}t\text{-}Bu)]_2(O)_2$ and $[Mn^{IV}(L\text{-}3\text{-}t\text{-}Bu)]_2(O)_2$.

Formation of Homochiral versus Heterochiral Dimers. Another point of stereochemical importance upon dimerization is the formation of homochiral versus heterochiral dimers from racemic monomers. It is well-known that a preferential formation of a homochiral over heterochiral dimers is important for nonlinear effects in asymmetric catalysis.[54] We then carried out a dimerization reaction of a racemic mixture containing equimolar (*R*,*R*)- and (*S*,*S*)-$Mn^{III}(L\text{-}3,5\text{-}t\text{-}Bu)(Cl)$. The ^{1}H NMR spectrum of the obtained product is identical to that of the product from the dimerization of enantiomerically pure (*R*,*R*)-$Mn^{III}(L\text{-}3,5\text{-}t\text{-}Bu)(Cl)$ (Figure S10, SI), suggesting that only the homochiral dimers are generated in the dimerization of racemic $Mn^{III}(L\text{-}3,5\text{-}t\text{-}Bu)(Cl)$.

To further confirm this result, we carried out a competitive dimerization reaction of (*S*,*S*)-$Mn^{III}(L\text{-}3,5\text{-}t\text{-}Bu)(Cl)$ with (*R*,*R*)-$Mn^{III}(L\text{-}3\text{-}t\text{-}Bu)(Cl)$ and analyzed the obtained mixture with ESI mass spectrometry (Figure 7a). When the dimerization is carried out for $Mn^{III}(L\text{-}3,5\text{-}t\text{-}Bu)(Cl)$ and $Mn^{III}(L\text{-}3\text{-}t\text{-}Bu)(Cl)$ with the same (*R*,*R*)-configuration, the obtained mixture affords the ion signal at *m*/*z* 1119.42 from the mixed dimer between $Mn^{III}(L\text{-}3,5\text{-}t\text{-}Bu)(Cl)$ and $Mn^{III}(L\text{-}3\text{-}t\text{-}Bu)(Cl)$ in addition to the ion signals at *m*/*z* 1007.24 and 1231.60 as a consequence of

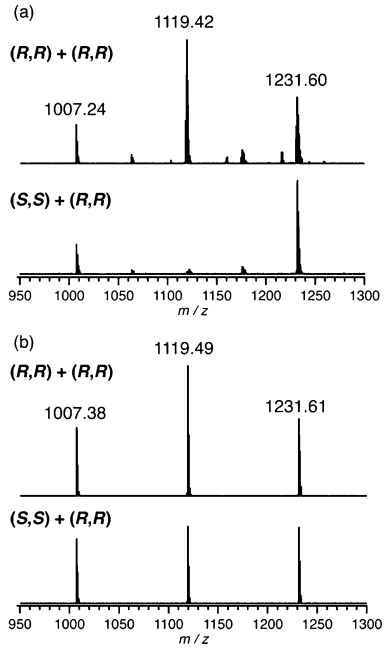

Figure 7. ESI mass spectra of the $[Mn^{IV}(salen)]_2(O)_2$ products (bottom) from (a) the competitive dimerization between (*S*,*S*)-$Mn^{III}(L\text{-}3,5\text{-}t\text{-}Bu)(Cl)$ and (*R*,*R*)-$Mn^{III}(L\text{-}3\text{-}t\text{-}Bu)(Cl)$, and (b) the competitive dimerization between (*S*,*S*)-$Mn^{III}(L\text{-}3,5\text{-}t\text{-}Bu)(Cl)$ and (*R*,*R*)-$Mn^{III}(L\text{-}5\text{-}t\text{-}Bu)(Cl)$. Reference spectra obtained from the reactions using $Mn^{III}(salen)(Cl)$ with the same (*R*,*R*)-configuration are shown for comparison (top).

dx.doi.org/10.1021/ic402572h | Inorg. Chem. 2014, 53, 1070−1079

homodimerizations (Figure 7a, top). In clear contrast, in the case of the dimerization between (*S*,*S*)-Mn^{III}(L-3,5-*t*-Bu)(Cl) and (*R*,*R*)-Mn^{III}(L-3-*t*-Bu)(Cl), the ion signal at *m*/*z* 1119.42 almost disappears (Figure 7a, bottom), which unambiguously indicates that the formation of the heterochiral dimer is significantly inhibited. Interestingly, when (*S*,*S*)-Mn^{III}(L-3,5-*t*-Bu)(Cl) is reacted with (*R*,*R*)-Mn^{III}(L-5-*t*-Bu)(Cl) instead of (*R*,*R*)-Mn^{III}(L-3-*t*-Bu)(Cl), the heterochiral dimer is generated as indicated by the appearance of the ion signal at 1119.49 (Figure 7b, bottom). This result clearly shows that the 3/3′-*tert*-butyl groups also play a pivotal role in directing the reaction to homochiral dimers over heterochiral dimers. Previously, Saito and Katsuki reported that their titanium salen complex preferentially forms a heterochiral dimer, leading to a positive nonlinear relation between the enantiomeric excesses of the catalyst and the products in asymmetric sulfoxidation.[55] The formation of a heterochiral versus a homochiral dimer is also utterly different between manganese and titanium.

The chiral Mn^{III}(L-3,5-*t*-Bu)(Cl) complex is a well-known enantioselective epoxidation catalyst, and the catalytic epoxidation reactions are carried out using NaOCl as an oxidant under CH_2Cl_2−H_2O biphasic conditions.[56] It is interesting to note that the aqueous solution is adjusted to basic conditions (pH = 11.3) by the addition of NaOH. The present $[Mn^{IV}$(L-3,5-*t*-Bu)$]_2(O)_2$ complex is readily formed under similar conditions by washing the toluene solution of Mn^{III}(L-3,5-*t*-Bu)(Cl) with aqueous KOH solution. To investigate a possible role of $[Mn^{IV}$(L-3,5-*t*-Bu)$]_2(O)_2$ in catalytic epoxidation, we carried out stoichiometric reactions of $[Mn^{IV}$(L-3,5-*t*-Bu)$]_2(O)_2$ with 1 equiv of *cis*-*β*-methylstyrene, thioanisole, and triphenylphosphine in CD_2Cl_2 (50 mM). However, ^{1}H NMR spectra show that the $[Mn^{IV}$(L-3,5-*t*-Bu)$]_2(O)_2$ complex remains intact after 1 day at room temperature in every case. We then attempted to use $[Mn^{IV}$(L-3,5-*t*-Bu)$]_2(O)_2$ as a catalyst for the epoxidation of *cis*-*β*-methylstyrene under exactly the same biphasic conditions using NaOCl as an oxidant,[56] but no epoxide product was obtained. Thus, the $[Mn^{IV}$(L-3,5-*t*-Bu)$]_2(O)_2$ complex is not an active oxygen atom transfer agent nor even a catalyst for epoxidation. The $[Mn^{IV}$(L-3,5-*t*-Bu)$]_2(O)_2$ complex could be converted back to a mixture of monomeric complexes containing catalytically active Mn^{III}(L-3,5-*t*-Bu)(Cl) by vigorously washing the solution with aqueous HCl solution, but under neutral and basic conditions, the $[Mn^{IV}$(L-3,5-*t*-Bu)$]_2(O)_2$ complex is quite stable. Thus, the formation of $[Mn^{IV}$(L-3,5-*t*-Bu)$]_2(O)_2$ leads to deactivation of this catalyst under basic epoxidation conditions using NaOCl as an oxidant.

DFT Studies. To investigate the origin of the difference between manganese and titanium, we systematically calculated optimized structures and energies for a set of di-*μ*-oxo dimetal complexes bearing different steric bulk as shown in Chart 3. Selected structural parameters and the energies are summarized in Tables S2−S5 (SI). In the case of di-*μ*-oxo dimanganese(IV) complexes, each manganese(IV) ion has three unpaired electrons, which are coupled to give quasi-degenerate multiple spin states. Among these spin states, the DFT results for the septet spin state are shown here. The experimental electronic structure of the di-*μ*-oxo dimanganese(IV) complex contains excited states in addition to the singlet ground state, as indicated from variable-temperature ^{1}H NMR spectra (Figure S3, SI). Among these computed structures, the *M*-helical di-*μ*-oxo dimanganese(IV) complex with L-3,5-*t*-Bu and *P*-helical di-*μ*-oxo dititanium(IV) complex with **3** are thoroughly compared with the corresponding X-ray crystal structures (Tables S6 and S7, SI). A satisfactory good agreement between experimental and calculated structural parameters (errors less than 6%) is observed for both cases using the LC-BLYP functional with the aug-cc-pVTZ basis set. We tested other functionals such as M062X and CAM-B3LYP and obtained consistent results for the energy difference between *M*- and *P*-helical dimers (Table S2, SI).

Optimized structures of *M*- and *P*-helical $[Mn^{IV}$(L-3,5-*t*-Bu)$]_2(O)_2$ and $[Ti^{IV}$(L-3,5-*t*-Bu)$]_2(O)_2$ are shown in Figure 8. In the case of manganese(IV), the *M*-helical dimer is predicted to be more stable than the *P*-helical dimer by 3.237 kcal mol^{-1}, which is in agreement with the experimental result. Computed structures show that the steric bulk at the 3/3′postion from two salen ligands causes severe steric repulsion for the *P*-helical dimer. Such interligand steric repulsion is weaker for the *M*-helical structure, because the change of the coordination site of the phenolate ligands separates the steric bulk at the 3/3′postion. Although the present experiment shows that the 3/3′-*tert*-butyl groups work as a key factor for the selective formation of the *M*-helical dimer, the computed energy difference between *M*- and *P*-helical $[Mn^{IV}$(L-3,5-*t*-Bu)$]_2(O)_2$ is rather small as compared with the energy difference between *M*- and *P*-helical di-*μ*-oxo dimanganese(IV) complexes with **3** in the absence of the *tert*-butyl groups (Tables S4 and S5, SI). Optimized structures in Figure 9 show that the di-*μ*-oxo dimanganese(IV) core of the computed *P*-helical $[Mn^{IV}$(L-3,5-*t*-Bu)$]_2(O)_2$ is considerably distorted, resulting in the elongation of the distance between the nearby phenolate rings. Such distortion is not observed for the other optimized di-*μ*-oxo dimanganese(IV) complexes in the absence of the 3/3′-*tert*-butyl groups. An unexpectedly small energy difference between *M*- and *P*-helical $[Mn^{IV}$(L-3,5-*t*-Bu)$]_2(O)_2$ is clearly a consequence of this distortion, which is probably caused by an underestimation of the destabilization energy to distort the di-*μ*-oxo dimanganese(IV) core with DFT calculations.

In clear contrast to the manganese case described above, the present DFT calculation indicates that the *P*-helical $[Ti^{IV}$(L-3,5-*t*-Bu)$]_2(O)_2$ complex is more stable than the *M*-helical $[Ti^{IV}$(L-3,5-*t*-Bu)$]_2(O)_2$ complex by 5.790 kcal mol^{-1}, which may account for the previous observation that the di-*μ*-oxo dititanium(IV) complex with L-3-*t*-Bu and **3** is *P*-helical. In *P*-helical $[Ti^{IV}$(L-3,5-*t*-Bu)$]_2(O)_2$, two salen complexes are significantly twisted to diminish the steric repulsion between the 3/3′-*tert*-butyl groups (Figure 8). As shown in Figure 9, the twist of two salen complexes in *P*-helical $[Ti^{IV}$(L-3,5-*t*-Bu)$]_2(O)_2$ comes from the distortion of the di-*μ*-oxo dititanium(IV) core in which the distance between the O atoms of the phenolates is more elongated than the distance between the N atoms of the azomethines. The distortion of the di-*μ*-oxo dititanium(IV) core is observed for *P*-helical di-*μ*-oxo dititanium(IV) complexes with **1**−**3** irrespective of the difference of steric bulk. It is also interesting to note that such distortion is not observed at all for the corresponding *P*-helical di-*μ*-oxo dimanganese(IV) com-

Chart 3

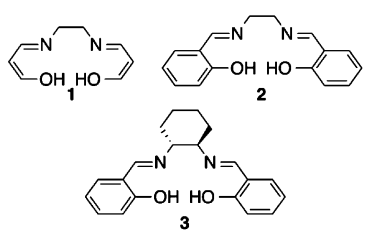

dx.doi.org/10.1021/ic402572h | Inorg. Chem. 2014, 53, 1070−1079

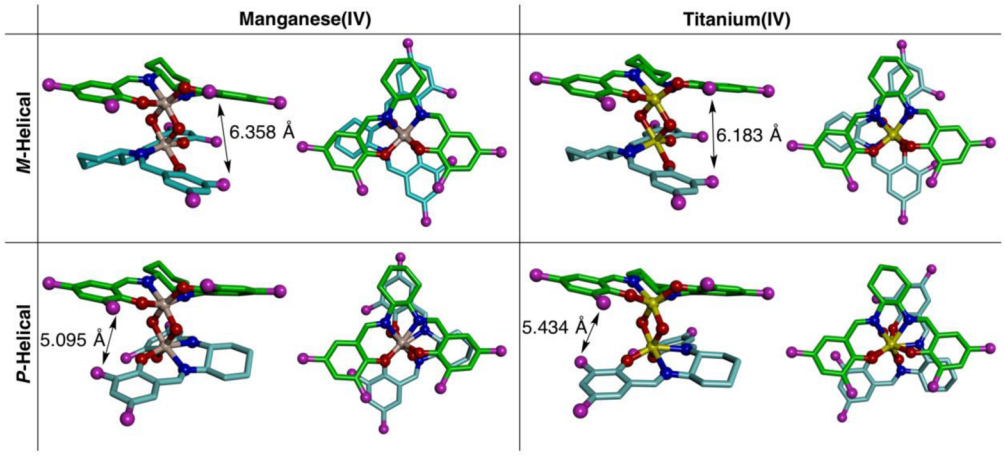

Figure 8. Computed structures for *M*- and *P*-helical $[Mn^{IV}(L\text{-}3,5\text{-}t\text{-}Bu)]_2(O)_2$ and $[Ti^{IV}(L\text{-}3,5\text{-}t\text{-}Bu)]_2(O)_2$. *M*-helical $[Mn^{IV}(L\text{-}3,5\text{-}t\text{-}Bu)]_2(O)_2$ is more stable than *P*-helical $[Mn^{IV}(L\text{-}3,5\text{-}t\text{-}Bu)]_2(O)_2$ by 3.237 kcal mol^{-1}. *P*-helical $[Ti^{IV}(L\text{-}3,5\text{-}t\text{-}Bu)]_2(O)_2$ is more stable than *M*-helical $[Ti^{IV}(L\text{-}3,5\text{-}t\text{-}Bu)]_2(O)_2$ by 5.790 kcal mol^{-1}. The LC-BLYP functional with the aug-cc-pVTZ basis set was utilized for DFT calculations.

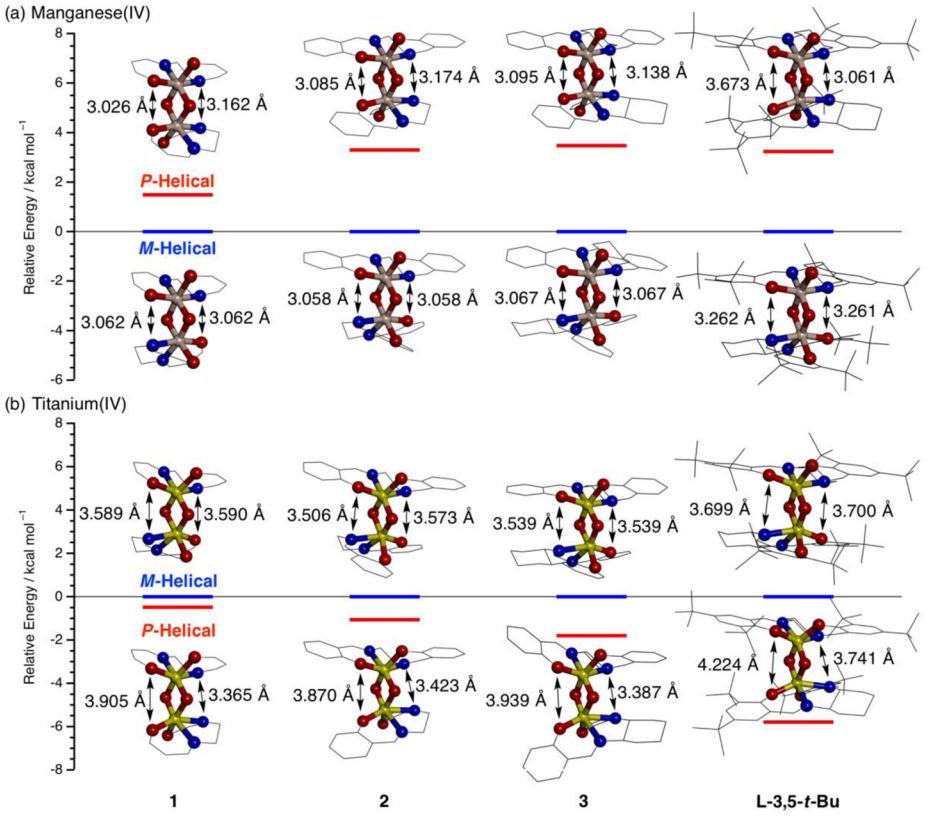

Figure 9. Difference of energy between *M*- and *P*-helical di-μ-oxo dimetal complexes with **1**−**3** and L-3,5-*t*-Bu. The LC-BLYP functional was utilized for DFT calculations.

plexes. This clearly indicates that the distorted di-μ-oxo dititanium(IV) cores originate in their electronic properties, not steric repulsion. We speculate that a larger degree of negative charge is induced on the oxygen atom next to Ti, because the Ti−O bond is less covalent than the Mn−O bond. Then, electrostatic repulsion elongates the distance between adjacent phenolate oxygen atoms, resulting in the distortion of the *P*-helical di-μ-oxo dititanium(IV) core. The distorted di-μ-oxo dititanium(IV) core provides a completely different framework for interligand interactions, as compared with the di-μ-oxo dimanganese(IV) core.

CONCLUSION

We herein describe diastereoselective assembly of chiral Mn^{III}(salen)(Cl) complexes via the di-μ-oxo dimanganese(IV) core. The present experiments and theoretical calculations show that the steric bulk at the 3/3′ position of the salicylidene ring plays a pivotal role in the diastereoselective formation of the *M*-helical dimer and the predominant formation of the homochiral dimer. This indicates that the di-μ-oxo dimanganese(IV) core provides a rigid framework for effective interligand steric interactions, which is a promising property as a building block to create coordination compounds with well-defined stereo-

dx.doi.org/10.1021/ic402572h | *Inorg. Chem.* 2014, 53, 1070−1079

chemistry. The present computational results also clarify that one of stereoisomeric di-μ-oxo dititanium(IV) cores with salen is significantly distorted as a consequence of the less covalent Ti−O bonding. This accounts for the striking difference between manganese and titanium in the stereochemistry upon dimerization. The present study thus reveals stereochemical aspects of the di-μ-oxo dimetal core, which are fundamentally important for the use of this unit.

EXPERIMENTAL SECTION

Instrumentation. HPLC purification was carried out using recycling preparative HPLC (LC-9201, Japan Analytical Industry). Absorption spectra were recorded in anhydrous CH_2Cl_2 using a quartz cell (l = 0.05 cm) on an Agilent 8453 spectrometer (Agilent Technologies) equipped with a Peltier-type temperature control unit. CD spectra were recorded in anhydrous CH_2Cl_2 using a quartz cell (l = 0.05 cm) on a J-720W spectropolarimeter (JASCO) equipped with a Peltier-type temperature control unit. NMR spectra (500 MHz) were measured in a borosilicate glass tube (O.D. = 5 mm) on an LA-500 spectrometer (JEOL). ^{1}H NMR chemical shifts in CD_2Cl_2 were referenced to $CHDCl_2$ (5.32 ppm). ESI-MS spectra were obtained with an LCT time-of-flight mass spectrometer equipped with an electrospray ionization interface (Micromass). Elemental analyses were conducted on a MICRO CORDER JM10 (J-SCIENCE LAB).

X-ray Crystallography. Measurements were made on a Rigaku/MSC Mercury CCD diffractometer equipped with the graphite monochromated Mo Kα radiation (λ = 0.71070 Å). Data were collected at 93 K under a cold nitrogen stream. All crystals were mounted on a glass fiber using epoxy glue. The images were processed with the CrystalClear program (ver. 1.3.6).[57] The structures were solved by the direct method using Sir2004[58] and refined by full-matrix least-squares procedures on F^2 using SHELXL,[59] on the CrystalStructure software package (ver. 4.0.1).[60] Anisotropic refinement was applied to all non-hydrogen atoms. Hydrogen atoms were placed at the calculated positions and refined with isotropic parameters. The Flack parameters[61] were calculated to confirm the absolute configuration. The thermal ellipsoid plot was generated by using Ortep-3 for Windows.[62] In the X-ray crystal structure of $[Mn^{IV}$(L-3,5-*t*-Bu)$]_2(O)_2$, the carbon atoms from flexible *tert*-butyl groups show considerably higher *U*eq values than those of the other carbon atoms from a rigid dinuclear framework. This causes a PLAT220 alert (level B) concerning *U*eq(max)/*U*eq(min) range for carbon atoms by the checkCIF service. The checkCIF service also points a PLAT306 alert (level B) concerning the test for isolated oxygen atoms, which is caused by a water molecule that is present as a solvent in the crystal. In spite of our effort to locate hydrogen atoms for a water molecule, we could not find hydrogen atoms from a difference map.

Materials. Anhydrous CH_2Cl_2 and DMF were purchased from Kanto or Wako and were utilized as received. CD_2Cl_2 was purchased from ACROS and was passed though aluminum oxide just before use. 3-*tert*-Butyl-2-hydroxybenzaldehyde, 5-*tert*-butyl-2-hydroxybenzaldehyde, and (*R*,*R*)-/(*S*,*S*)-*N*,*N*′-bis(3,5-di-*tert*-butylsalicylidene)-1,2-cyclohexanediaminomanganese(III) chloride were purchased from Aldrich and were used as received. (*R*,*R*)-1,2-Cyclohexanediamine was purchased from Tokyo Chemical Industry and was utilized as received. Manganese(II) acetate tetrahydrate was purchased from Wako. The preparation of selectively deuterated salen ligands (L-3,5-*t*-Bu-d_2 and L-3,5-*t*-Bu-d_4 in Chart 2) were reported previously.[50,63]

Synthesis of Mn^{III}(L-3-*t*-Bu)(Cl). The solution of (*R*,*R*)-1,2-cyclohexanediamine (1.450 g, 12.7 mmol) in anhydrous DMF (6 mL) was added to the solution of 3-*tert*-butyl-2-hydroxybenzaldehyde (4.525 g, 25.4 mmol) in anhydrous DMF (6 mL). The resulting solution was heated at 100 °C for 30 min. Then, at room temperature, 1.1 equiv of $Mn_2(OAc)_2{\cdot}4H_2O$ (3.422 g, 14.0 mmol) was added to the solution. The resulting mixture was heated at 100 °C for 2 h until the metal-free salen ligand was not detected with thin-layer chromatography. The DMF solvent was removed in vacuo. The residue was dissolved in EtOH (20 mL) and was then precipitated by the addition of aqueous HCl solution (1 M, 80 mL) to remove a trace of DMF. The resulting solid dissolved in CH_2Cl_2 (100 mL) was washed with aqueous HCl solution (1 M, 50 mL × 2). The CH_2Cl_2 layer was dried over $MgSO_4$, and then the solvent was removed by evaporation under reduced pressure. The residue dissolved in CH_2Cl_2 (10 mL) was passed through a membrane filter (Millex-FG, pore size 0.20 μm, diameter 25 mm, Millipore). The addition of hexane afforded Mn^{III}(L-3-*t*-Bu)(Cl) (4.88 g, 9.30 mmol) as a brown solid in a 73% yield after drying in vacuo at 100 °C for 12 h. Anal. Calcd for $C_{28}H_{36}ClMnN_2O_2{\cdot}(H_2O)_{0.1}$: C, 64.08; H, 6.95; N, 5.34. Found: C, 64.11; H, 6.90; N, 5.36.

Synthesis of Mn^{III}(L-5-*t*-Bu)(Cl). The solution of (*R*,*R*)-1,2-cyclohexanediamine (315 mg, 2.8 mmol) in anhydrous DMF (3 mL) was added to the solution of 5-*tert*-butyl-2-hydroxybenzaldehyde (982 mg, 5.5 mmol) in anhydrous DMF (1 mL). The resulting solution was heated at 100 °C for 30 min. Then, at room temperature, 1.1 equiv of $Mn_2(OAc)_2{\cdot}4H_2O$ (743 mg, 3.0 mmol) was added to the solution. The resulting mixture was heated at 100 °C for 2 h until the metal-free salen ligand was not detected with thin-layer chromatography. The DMF solvent was removed in vacuo. The residue was dissolved in acetone (5 mL) and was then precipitated by the addition of aqueous HCl solution (1 M, 60 mL). The precipitate was once again dissolved in acetone (10 mL) and was precipitated by the addition of aqueous HCl solution (1 M, 60 mL). After drying in vacuo, the resulting solid dissolved in CH_2Cl_2 (5 mL) was passed through a membrane filter (Millex-FG, pore size 0.20 μm, diameter 25 mm, Millipore). The addition of hexane afforded Mn^{III}(L-5-*t*-Bu)(Cl) (911 mg, 1.7 mmol) as a brown solid in a 62% yield after drying in vacuo at 100 °C for 12 h. Anal. Calcd for $C_{28}H_{36}ClMnN_2O_2$: C, 64.30; H, 6.94; N, 5.36. Found: C, 64.38; H, 6.84; N, 5.39.

Synthesis of $[Mn^{IV}$(L-3,5-*t*-Bu)$]_2(O)_2$. The solution of Mn^{III}(L-3,5-*t*-Bu)(Cl) (1 g, 1.57 mmol) in toluene (40 mL) was vigorously washed with aqueous KOH solution (2 M, 40 mL). The toluene layer was dried over $MgSO_4$, and then the solvent was removed by evaporation under reduced pressure. After drying in vacuo, the residue, dissolved in toluene (5 mL), was passed through a membrane filter (Millex-FG, pore size 0.20 μm, diameter 25 mm, Millipore). After removing the solvent and drying the residue in vacuo, anhydrous CH_3CN (30 mL) was added. The resulting suspension was heated at 90 °C for 1 h. The hot suspension was then filtered to afford analytically pure $[Mn^{IV}$(L-3,5-*t*-Bu)$]_2(O)_2$ (694 mg, 0.56 mmol) as a brown solid in a 71% yield, after drying in vacuo at room temperature. The crystal suitable for X-ray crystallography was obtained by letting stand the saturated CH_3CN solution (~10 mg in 20 mL) at 40 °C. Anal. Calcd for $C_{72}H_{106}Mn_2N_4O_7{\cdot}H_2O$: C, 69.21; H, 8.55; N, 4.48. Found: C, 69.11; H, 8.47; N, 4.51.

Synthesis of $[Mn^{IV}$(L-3-*t*-Bu)$]_2(O)_2$. The solution of Mn^{III}(L-3-*t*-Bu)(Cl) (700 mg, 1.33 mmol) in toluene (30 mL) and CH_2Cl_2 (10 mL) was vigorously washed with aqueous KOH solution (2 M, 100 mL). The organic layer was dried over $MgSO_4$, and then the solvent was removed by evaporation under reduced pressure. After drying in vacuo, the residue, dissolved in toluene (5 mL), was passed through a membrane filter (Millex-FG, pore size 0.20 mm, diameter 25 mm, Millipore). The solvent was removed, and the resulting residue was dried in vacuo. The residue was purified by HPLC (LC-9201, Japan Analytical Industry) using $CHCl_3$ containing 3% Et_3N to remove the metal-free ligand as a byproduct. Finally, to remove $Et_3N{\cdot}HCl$, the sample, dissolved in toluene (15 mL), was washed with saturated aqueous $NaHCO_3$ solution (60 mL). The solvent was removed by evaporation under reduced pressure, and the product was dried in vacuo. The residue dissolved in CH_2Cl_2 (3 mL) was passed through a membrane filter (Millex-FG, pore size 0.45 μm, diameter 13 mm, Millipore). The addition of hexane afforded $[Mn^{IV}$(L-3-*t*-Bu)$]_2(O)_2$ (33 mg, 0.033 mmol) as a brown solid in a 5% yield after drying in vacuo at room temperature. Anal. Calcd for $C_{56}H_{72}Mn_2N_4O_6{\cdot}(H_2O)_{0.1}$: C, 66.67; H, 7.21; N, 5.55. Found: C, 66.61; H, 7.20; N, 5.52.

Synthesis of $[Mn^{IV}$(L-5-*t*-Bu)$]_2(O)_2$. The solution of Mn^{III}(L-5-*t*-Bu)(Cl) (736 mg, 1.41 mmol) in CH_2Cl_2 (100 mL) was vigorously washed with aqueous KOH solution (2 M, 100 mL). The organic layer was dried over $MgSO_4$, and then the solvent was removed by evaporation under reduced pressure. After drying in vacuo, the residue dissolved in CH_2Cl_2 (5 mL) was passed through a membrane filter (Millex-FG, pore size 0.20 mm, diameter 25 mm, Millipore). The

dx.doi.org/10.1021/ic402572h | Inorg. Chem. 2014, 53, 1070−1079

solvent was removed, and the resulting residue was dried in vacuo. The residue was dissolved in CH_2Cl_2 (2 mL), and the addition of hexane (40 mL) afforded brown precipitate (625 mg, 0.59 mmol, 84%) that is characterized as a mixture of diastereomeric $[Mn^{IV}(L\text{-}5\text{-}t\text{-}Bu)]_2(O)_2$ complexes. Anal. Calcd for $C_{56}H_{72}Mn_2N_4O_6\cdot(H_2O)_{2.6}$: C, 63.82; H, 7.38; N, 5.32. Found: C, 63.79; H, 7.08; N, 5.35.

The diastereomeric $[Mn^{IV}(L\text{-}5\text{-}t\text{-}Bu)]_2(O)_2$ complexes (200 mg) were separated by HPLC (LC-9201, Japan Analytical Industry) using $CHCl_3$ containing 3% Et_3N. To remove Et_3N·HCl, the sample dissolved in toluene (15 mL) was washed with saturated aqueous $NaHCO_3$ solution (60 mL). The solvent was removed by evaporation under reduced pressure, and the product was dried in vacuo. The residue dissolved in CH_2Cl_2 (3 mL) was passed through a membrane filter (Millex-FG, pore size 0.45 μm, diameter 13 mm, Millipore). The addition of hexane afforded *M*-helical $[Mn^{IV}(L\text{-}5\text{-}t\text{-}Bu)]_2(O)_2$ (58 mg) and *P*-helical $[Mn^{IV}(L\text{-}5\text{-}t\text{-}Bu)]_2(O)_2$ (23 mg), after drying in vacuo at room temperature. *P*-helical dimer (minor component): Anal. Calcd for $C_{56}H_{72}Mn_2N_4O_6\cdot(H_2O)_{3.4}$: C, 62.96; H, 7.43; N, 5.24. Found: C, 62.76; H, 7.13; N, 5.18. *M*-helical dimer (major component): Anal. Calcd for $C_{56}H_{72}Mn_2N_4O_6\cdot(H_2O)_{2.6}$: C, 63.82; H, 7.38; N, 5.32. Found: C, 63.78; H, 7.31; N, 5.35.

Competitive Dimerization. An equimolar mixture of (*S*,*S*)-Mn^{III}(L-3,5-*t*-Bu)(Cl) (200 mg, 0.32 mmol) and (*R*,*R*)-Mn^{III}(L-3-*t*-Bu)(Cl) (165 mg, 0.32 mmol) was dissolved in toluene (15 mL) and CH_2Cl_2 (5 mL). The resulting solution was vigorously washed with aqueous KOH solution (2 M, 50 mL). The organic layer was dried over $MgSO_4$, and then the solvent was removed by evaporation under reduced pressure. After drying in vacuo, the residue dissolved in toluene (5 mL) was passed through a membrane filter (Millex-FG, pore size 0.20 mm, diameter 25 mm, Millipore). The solvent was removed, and the resulting residue was dried in vacuo. The product dissolved in CH_2Cl_2 was analyzed with ESI mass spectrometer. The other competitive dimerization reactions were carried out in the same manner.

DFT Calculations. DFT calculation was performed using the Gaussian 09 program package. The optimized structures and the vibrational frequencies were calculated using the LC-BLYP functional with the aug-cc-pVTZ basis set.

■ ASSOCIATED CONTENT

Supporting Information

Figures S1−S10 and Tables S1−S7. This material is available free of charge via the Internet at http://pubs.acs.org.

■ AUTHOR INFORMATION

Corresponding Author

*E-mail: hiro@ims.ac.jp.

Notes

The authors declare no competing financial interest.

■ ACKNOWLEDGMENTS

This work was supported by grants from Japan Society for the Promotion of Science (Grant-in-Aid for Scientific Research, Grant Nos. 25288032 and 23550086).

■ REFERENCES

(1) Wu, A. J.; Penner-Hahn, J. E.; Pecoraro, V. L. *Chem. Rev.* **2004**, *104*, 903−938.
(2) Mukhopadhyay, S.; Mandal, S. K.; Bhaduri, S.; Armstrong, W. H. *Chem. Rev.* **2004**, *104*, 3981−4026.
(3) Mullins, C. S.; Pecoraro, V. L. *Coord. Chem. Rev.* **2008**, *252*, 416−443.
(4) Cady, C. W.; Crabtree, R. H.; Brudvig, G. W. *Coord. Chem. Rev.* **2008**, *252*, 444−455.
(5) Que, L., Jr.; Tolman, W. B. *Angew. Chem., Int. Ed.* **2002**, *41*, 1114−1137.
(6) Tshuva, E. Y.; Lippard, S. J. *Chem. Rev.* **2004**, *104*, 987−1012.
(7) Mirica, L. M.; Ottenwaelder, X.; Stack, T. D. P. *Chem. Rev.* **2004**, *104*, 1013−1045.
(8) Lewis, E. A.; Tolman, W. B. *Chem. Rev.* **2004**, *104*, 1047−1076.
(9) Knof, U.; von Zelewsky, A. *Angew. Chem., Int. Ed.* **1999**, *38*, 302−322.
(10) Mateos-Timoneda, M. A.; Crego-Calama, M.; Reinhoudt, D. N. *Chem. Soc. Rev.* **2004**, *33*, 363−372.
(11) Albrecht, M. *Angew. Chem., Int. Ed.* **2005**, *44*, 6448−6451.
(12) Crassous, J. *Chem. Soc. Rev.* **2009**, *38*, 830−845.
(13) Keene, F. R. *Dalton Trans.* **2011**, *40*, 2405−2418.
(14) Howson, S. E.; Scott, P. *Dalton Trans.* **2011**, *40*, 10268−10277.
(15) Dong, Z.; Karpowicz, R. J., Jr.; Bai, S.; Yap, G. P. A.; Fox, J. M. *J. Am. Chem. Soc.* **2006**, *128*, 14242−14243.
(16) Heo, J.; Jeon, Y.-M.; Mirkin, C. A. *J. Am. Chem. Soc.* **2007**, *129*, 7712−7713.
(17) Miyake, H.; Kamon, H.; Miyahara, I.; Sugimoto, H.; Tsukube, H. *J. Am. Chem. Soc.* **2008**, *130*, 792−793.
(18) Rang, A.; Engeser, M.; Maier, N. M.; Nieger, M.; Lindner, W.; Schalley, C. A. *Chem.—Eur. J.* **2008**, *14*, 3855−3859.
(19) Gregolinski, J.; Starynowicz, P.; Hua, K. T.; Lunkley, J. L.; Muller, G.; Lisowski, J. *J. Am. Chem. Soc.* **2008**, *130*, 17761−17773.
(20) Sharma, S.; Lombeck, F.; Eriksson, L.; Johansson, O. *Chem.—Eur. J.* **2010**, *16*, 7078−7081.
(21) Albrecht, M.; Isaak, E.; Baumert, M.; Gossen, V.; Raabe, G.; Fröhlich, R. *Angew. Chem., Int. Ed.* **2011**, *50*, 2850−2853.
(22) Akine, S.; Hotate, S.; Nabeshima, T. *J. Am. Chem. Soc.* **2011**, *133*, 13868−13871.
(23) Yuasa, J.; Ohno, T.; Miyata, K.; Tsumatori, H.; Hasegawa, Y.; Kawai, T. *J. Am. Chem. Soc.* **2011**, *133*, 9892−9902.
(24) Ousaka, N.; Takeyama, Y.; Iida, H.; Yashima, E. *Nat. Chem.* **2011**, *3*, 856−861.
(25) Howson, S. E.; Bolhuis, A.; Brabec, V.; Clarkson, G. J.; Malina, J.; Rodger, A.; Scott, P. *Nat. Chem.* **2012**, *4*, 31−36.
(26) Ousaka, N.; Grunder, S.; Castilla, A. M.; Whalley, A. C.; Stoddart, J. F.; Nitschke, J. R. *J. Am. Chem. Soc.* **2012**, *134*, 15528−15537.
(27) McGarrigle, E. M.; Gilheany, D. G. *Chem. Rev.* **2005**, *105*, 1563−1602.
(28) Darensbourg, D. J. *Chem. Rev.* **2007**, *107*, 2388−2410.
(29) Miyasaka, H.; Saitoh, A.; Abe, S. *Coord. Chem. Rev.* **2007**, *251*, 2622−2664.
(30) Wezenberg, S. J.; Kleij, A. W. *Angew. Chem., Int. Ed.* **2008**, *47*, 2354−2364.
(31) Larson, E. J.; Pecoraro, V. L. *J. Am. Chem. Soc.* **1991**, *113*, 3810−3818.
(32) Gohdes, J. W.; Armstrong, W. H. *Inorg. Chem.* **1992**, *31*, 368−373.
(33) Larson, E.; Lah, M. S.; Li, X.; Bonadies, J. A.; Pecoraro, V. L. *Inorg. Chem.* **1992**, *31*, 373−378.
(34) Torayama, H.; Nishide, T.; Asada, H.; Fujiwara, M.; Matsushita, T. *Polyhedron* **1998**, *17*, 105−118.
(35) Law, N. A.; Kampf, J. W.; Pecoraro, V. L. *Inorg. Chim. Acta* **2000**, *297*, 252−264.
(36) Belokon', Y. N.; Caveda-Cepas, S.; Green, B.; Ikonnikov, N. S.; Khrustalev, V. N.; Larichev, V. S.; Moscalenko, M. A.; North, M.; Orizu, C.; Tararov, V. I.; Tasinazzo, M.; Timofeeva, G. I.; Yashkina, L. V. *J. Am. Chem. Soc.* **1999**, *121*, 3968−3973.
(37) Tararov, V. I.; Larichev, V. S.; Moscalenko, M. A.; Yashkina, L. V.; Khrustalev, V. N.; Antipin, M. Y.; Börner, A.; Belokon', Y. N. *Enantiomer* **2000**, *5*, 169−173.
(38) Tsuchimoto, M. *Bull. Chem. Soc. Jpn.* **2001**, *74*, 2101−2105.
(39) Belokon', Y. N.; Blacker, A. J.; Carta, P.; Clutterbuck, L. A.; North, M. *Tetrahedron* **2004**, *60*, 10433−10447.
(40) Davis, A.; Kilner, C. A.; Kee, T. P. *Inorg. Chim. Acta* **2004**, *357*, 3493−3502.
(41) Matsumoto, K.; Sawada, Y.; Saito, B.; Sakai, K.; Katsuki, T. *Angew. Chem., Int. Ed.* **2005**, *44*, 4935−4939.
(42) Gibson, V. C.; Gregson, C. K. A.; Halliwell, C. M.; Long, N. J.; Oxford, P. J.; White, A. J. P.; Williams, D. J. *J. Organomet. Chem.* **2005**, *690*, 6271−6283.

(43) Sawada, Y.; Matsumoto, K.; Kondo, S.; Watanabe, H.; Ozawa, T.; Suzuki, K.; Saito, B.; Katsuki, T. *Angew. Chem., Int. Ed.* **2006**, *45*, 3478−3480.
(44) Belokon', Y. N.; Clegg, W.; Harrington, R. W.; North, M.; Young, C. *Inorg. Chem.* **2008**, *47*, 3801−3814.
(45) Kondo, S.; Saruhashi, K.; Seki, K.; Matsubara, K.; Miyaji, K.; Kubo, T.; Matsumoto, K.; Katsuki, T. *Angew. Chem., Int. Ed.* **2008**, *47*, 10195−10198.
(46) Manna, C. M.; Armony, G.; Tshuva, E. Y. *Inorg. Chem.* **2011**, *50*, 10284−10291.
(47) For the nomenclature of octahedral geometries with tetradentate ligands, see ref 9.
(48) Berova, N.; Nakanishi, K.; Woody, R. W. *Circular Dichroism: Principles and Applications*; Wiley-VCH: New York, 2000; Vol. *2*.
(49) Berova, N.; Di Bari, L.; Pescitelli, G. *Chem. Soc. Rev.* **2007**, *36*, 914−931.
(50) Kurahashi, T.; Hada, M.; Fujii, H. *J. Am. Chem. Soc.* **2009**, *131*, 12394−12405.
(51) Kurahashi, T.; Fujii, H. *Inorg. Chem.* **2008**, *47*, 7556−7567.
(52) Wang, C.; Kurahashi, T.; Fujii, H. *Angew. Chem., Int. Ed.* **2012**, *51*, 7809−7811.
(53) Telfer, S. G.; Tajima, N.; Kuroda, R. *J. Am. Chem. Soc.* **2004**, *126*, 1408−1418.
(54) Girard, C.; Kagan, H. B. *Angew. Chem., Int. Ed.* **1998**, *37*, 2922−2959.
(55) Saito, B.; Katsuki, T. *Tetrahedron Lett.* **2001**, *42*, 8333−8336.
(56) Jacobsen, E. N.; Zhang, W.; Muci, A. R.; Ecker, J. R.; Deng, L. *J. Am. Chem. Soc.* **1991**, *113*, 7063−7064.
(57) *CrystalClear*: An Integrated Program for the Collection and Processing of Area Detector Data;Rigaku Corporation: Tokyo, Japan, 2006.
(58) Burla, M. C.; Caliandro, R.; Camalli, M.; Carrozzini, B.; Cascarano, G. L.; De Caro, L.; Giacovazzo, C.; Polidori, G.; Spagna, R. *J. Appl. Crystallogr.* **2005**, *38*, 381−388.
(59) Sheldrick, G. M. *Acta Crystallogr., Sect. A* **2008**, *64*, 112−122.
(60) *CrystalStructure: Crystal Structure Analysis Package*; Rigaku Corporation: Tokyo, Japan, 2010.
(61) Flack, H. D. *Acta Crystallogr., Sect. A* **1983**, *39*, 876−881.
(62) Farrugia, L. J. *J. Appl. Crystallogr.* **1997**, *30*, 565−565.
(63) Kurahashi, T.; Fujii, H. *J. Am. Chem. Soc.* **2011**, *133*, 8307−8316.